CrossMark

HARD X-RAY EMISSION FROM SH 2-104: A *NuSTAR* SEARCH FOR GAMMA-RAY COUNTERPARTS

E. V. GOTTHELF[1,2], K. MORI[1], E. ALIU[2], J. M. PAREDES[2], J. A. TOMSICK[3], S. E. BOGGS[3], F. E. CHRISTENSEN[4], W. W. CRAIG[3,5], C. J. HAILEY[1], F. A. HARRISON[6], J. S. HONG[7], F. RAHOUI[8,11], D. STERN[9], AND W. W. ZHANG[10]

[1] Columbia Astrophysics Laboratory, Columbia University, 550 West 120th Street, New York, NY 10027-6601, USA; eric@astro.columbia.edu
[2] Departament de Física Quàntica i Astrofísica, Institut de Ciències del Cosmos, Universitat de Barcelona, IEEC-UB, Martí i Franquès 1, E-08028, Barcelona, Spain
[3] Space Sciences Laboratory, University of California, Berkeley, CA 94720, USA
[4] DTU Space-National Space Institute, Technical University of Denmark, Elektrovej 327, DK-2800 Lyngby, Denmark
[5] Lawrence Livermore National Laboratory, Livermore, CA 94550, USA
[6] Cahill Center for Astronomy and Astrophysics, California Institute of Technology, Pasadena, CA 91125, USA
[7] Harvard-Smithsonian Center for Astrophysics, Cambridge, MA 02138, USA
[8] Department of Astronomy, Harvard University, 60 Garden Street, Cambridge, MA 02138, USA
[9] Jet Propulsion Laboratory, California Institute of Technology, 4800 Oak Grove Drive, Pasadena, CA 91109, USA
[10] NASA Goddard Space Flight Center, Greenbelt, MD 20771, USA
[11] European Southern Observatory, Karl Schwarzschild-Strasse 2, D-85748 Garching bei München, Germany
Received 2016 February 2; revised 2016 April 21; accepted 2016 May 8; published 2016 July 18

ABSTRACT

We present *NuSTAR* hard X-ray observations of Sh 2–104, a compact H II region containing several young massive stellar clusters (YMSCs). We have detected distinct hard X-ray sources coincident with localized VERITAS TeV emission recently resolved from the giant gamma-ray complex MGRO J2019+37 in the Cygnus region. Fainter, diffuse X-rays coincident with the eastern YMSC in Sh2-104 likely result from the colliding winds of a component star. Just outside the radio shell of Sh 2–104 lies 3XMM J201744.7+365045 and a nearby nebula, NuSTAR J201744.3+364812, whose properties are most consistent with extragalactic objects. The combined *XMM-Newton* and *NuSTAR* spectrum of 3XMM J201744.7+365045 is well-fit to an absorbed power-law model with $N_{\rm H} = (3.1 \pm 1.0) \times 10^{22}\,{\rm cm}^{-2}$ and a photon index $\Gamma = 2.1 \pm 0.1$. Based on possible long-term flux variation and the lack of detected pulsations ($\leqslant 43\%$ modulation), this object is likely a background active galactic nucleus rather than a Galactic pulsar. The spectrum of the *NuSTAR* nebula shows evidence of an emission line at $E = 5.6\,{\rm keV}$, suggesting an optically obscured galaxy cluster at $z = 0.19 \pm 0.02$ ($d = 800$ Mpc) and $L_X = 1.2 \times 10^{44}\,{\rm erg\,s}^{-1}$. Follow-up *Chandra* observations of Sh 2–104 will help identify the nature of the X-ray sources and their relation to MGRO J2019+37. We also show that the putative VERITAS excess south of Sh 2–104, is most likely associated with the newly discovered *Fermi* pulsar PSR J2017+3625 and not the H II region.

Key words: ISM: individual objects (Sh 2-104, MGRO J2019+37, 3XMM J201744.7+365045, VER J2019+368) – pulsars: individual (NuSTAR J201744.3+364812) – stars: neutron

1. INTRODUCTION

MGRO J2019+37 is the brightest Milagro gamma-ray source in the Cygnus region, with 80% of the Crab Nebula flux at 20 TeV (Abdo et al. 2007). The origin and nature of MGRO J2019+37 has long been the subject of debate as its ∼1° extent overlaps several supernova remnants, H II regions, Wolf-Rayet stars, >100 MeV gamma-ray sources, one or more *Fermi* pulsars, and a hard X-ray transient. Recent TeV observations on ∼6′ scales using the VERITAS telescope clearly resolve the giant gamma-ray complex into at least three distinct TeV emission regions, each coincident with a *Fermi* source (Aliu et al. 2014). The bulk of the VERITAS emission from MGRO J2019+37 falls into the elongated ($1°.1 \times 0°.6$), spectrally distinct (harder) source VER J2019+368 (see Figure 1).

Paredes et al. (2009) argues that the *Fermi* pulsar PSR J2021+3651 (Roberts et al. 2002) at the eastern edge of VER J2019+368 is not sufficiently energetic to power all the gamma-ray flux in the region based on the time required for electrons to diffuse and fill the large emitting volume relative to their cooling lifetime. Instead, these authors suggest that massive star-forming activity associated with the H II region Sharpless 104 (herein Sh 2–104) can contribute to the gamma-ray flux from VER J2019+368, possibly through wind collisions or interactions of protostar jets with the surrounding medium (Torres et al. 2004).

The well-studied Sh 2–104 lies beyond the Cygnus galactic arm, 4.0 ± 0.5 kpc away, and contains at least two ultra compact massive stellar clusters within its ∼7′ radio diameter (Paredes et al. 2009). The massive CO clouds around the star clusters suggest Sh 2–104 is a prototype of massive star formation triggered by the expansion of a H II region (Deharveng et al. 2003). An associated H-alpha nebula is clearly resolved in the DSS POSSII-J image, likely powered by a central O6 V star ionizing the region (Lahulla 1985) and possibly a bright nearby IRAS source.

A serendipitous *XMM-Newton* observation of the MGRO J2019+37 field caught the eastern half of the Sh 2–104 radio shell at the edge of the field of view. Image analysis by Zabalza et al. (2010) revealed faint emission in this short exposure (20 ks), just above the noise level, which suggested several point sources within the radio shell. Most notably, these include ones overlapping the central star, coincident with a 2σ ROSAT source, and the eastern young massive stellar cluster (YMSC). Just outside the radio shell lies 3XMM J201744.7+365045 and a barely detected nebula ∼2′ in diameter. These results open the possibility of identifying a low-energy counterpart to the gamma-ray emission and help identify its origin.

As part of the *NuSTAR* Galactic Survey program we have obtained broad band X-ray observations of Sh 2–104. In this paper, we report the detection of hard X-ray emission from the
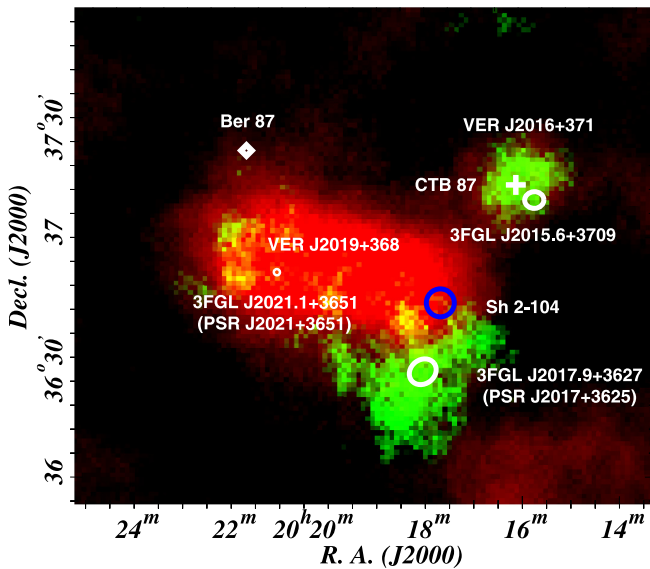
Figure 1. TeV gamma-ray map of the MGRO J2019+37 region resolved into distinct sources using VERITAS observations. Note that the Milagro source itself fills the field of view. Superimposed are VERITAS images in two energy bands, 0.6–1 TeV (green) and >1 TeV (red), that clearly separate the Milagro emission into at least three distinct emission components, each associated with a *Fermi* source (white circles). The harder, extended TeV emission, VER J2019 +368, is associated with the pulsar PSR J2021+3651; Sh 2–104, denoted by the blue circle, may contribute a western component of this emission. Modified from Aliu et al. (2014).

eastern YMSC and from the *XMM-Newton* source and the nearby diffuse nebula. We consider the possibility that these sources are related to the star formation regions and/or associated with gamma-ray emission. Alternatively, the latter two sources may have an unrelated extragalactic origin.

2. NuSTAR OBSERVATIONS OF SH 2–104

NuSTAR observed the H II region Sh 2–104 on 2014 October 21 (ObsId #30001048) followed by a second overlapping observation, offset to the south, on 2014 November 13 (ObsId #30001049). *NuSTAR* consists of two co-aligned X-ray telescopes, with corresponding focal plane modules, FPMA and FPMB, that provide 18′ FWHM imaging resolution over a 3–79 keV X-ray band, with a characteristic spectral resolution of 400 eV FWHM at 10 keV (Harrison et al. 2013). The reconstructed *NuSTAR* coordinates are accurate to 7″.5 at the 90% confidence level. The relative timing accuracy of *NuSTAR* is ∼2 ms rms after correcting for thermal drift of the on-board clock, with the absolute timescale shown to be better than <3 ms (Mori et al. 2014; Madsen et al. 2015).

The data were processed and analyzed using FTOOLS 24Jan2014_V6.15.1 (NUSTARDAS 09Dec13_v1.3.1) with *NuSTAR* Calibration Database (CALDB) files from 2013 August 30. The resulting data set provides a total of 80.5 ks and 91.6 ks of net good time for the two pointings, respectively, after removing intervals of high background rates. We also exclude a bright arc of stay light that contaminates the eastern edge of the field of view in both detectors during the first observation. The extracted spectra combined data from both FPM detectors, grouped into appropriate spectral fitting channels and modeled using the XSPEC (v12.8.2) spectral fitting package (Arnaud 1996). All spectral fits use the TBabs absorption model in XSPEC with the Wilms solar abundances

(Wilms et al. 2000) and the Verner photoionization cross-section (Verner et al. 1996).

2.1. Image Analysis

Figure 2 presents the exposure-corrected 3–79 keV *NuSTAR* images of the Sh 2–104 field, combining data from both FPM detectors. The images are smoothed using a $\sigma = 3''.7$ Gaussian kernel and scaled linearly. Most prominently, we detect a hard (>30 keV) point source just north of the Sh 2–104 complex and a poorly resolved nebula 2′.3 below it, roughly 2′.4 in diameter. These sources clearly correspond to faint X-ray emission seen in a short, 20 ks, 2007 *XMM-Newton* observation, detected serendipitously, at the very edge of the field of view (Zabalza et al. 2010).

The two bright *NuSTAR* sources are embedded in enhanced diffuse emission that overlaps, at least in part, with the Sh 2–104 radio nebula. Of particular interest is a faint nebula detected at the radio spur of Sh 2–104, coincident with the eastern YMSC discussed in Paredes et al. (2009). Its spatial extent of $r \sim 0'.5$, corrected for the PSF, is consistent with the size of the optical cluster. Farther south we find evidence of several other faint sources including a *Swift* X-ray source obtained as part of the follow-up program of *Fermi* sources. Table 1 presents the list of detected *NuSTAR* sources along with the significance of detection computed by wavdetect. The source coordinates are accurate to ≈4″.0, registered using 3XMM J201744.7+365045, the counterpart to the bright *NuSTAR* point source. Finally, we note that no hard X-ray counterpart is detected for the *ROSAT* source at the center of Sh 2–104 (Paredes et al. 2009). This suggest a soft X-ray source, likely thermal emission from the bright star in the central cluster, or a low-temperature colliding wind binary within this cluster.

2.2. Spectral Analysis

To preface our spectral analysis we note that the *NuSTAR* low-energy response (3 keV) is too hard to constrain the absorbing column for a typical source with $N_H < 10^{22}$ cm^{-2}. In the following spectral fits using *NuSTAR* data alone, for definitiveness, we hold the column density fixed to a fiducial value of the Galactic total. Generally, the range of likely column density here is found to have no significant effect on the resulting spectral parameters. We include both a neutral hydrogen[12] and a molecular hydrogen component to the column density to take into account significant local CO emission (see Dame et al. 2001). We compute a total Galactic column density of $N_H = n_{H I} + 2n_{H_2} = 2.4 \times 10^{22}$ cm^{-2}, a value consistent with the results of the combined *XMM-Newton* and *NuSTAR* fit to the spectrum of 3XMM J201744.7+365045 presented below. In all cases, the quoted spectral uncertainties are at the 90% confidence level for one or two interesting parameter(s) for the one- and two-component spectral fits, respectively.

The high-energy emission from the eastern YMSC is of great interest, as this source is a natural candidate for the observed gamma-ray emission. We extracted a *NuSTAR* spectrum from the YMSC using an $r < 0'.8$ aperture in the usable 3–10 keV range. This yields a total of 680 counts of which 71% are from background contamination, as estimated from counts extracted
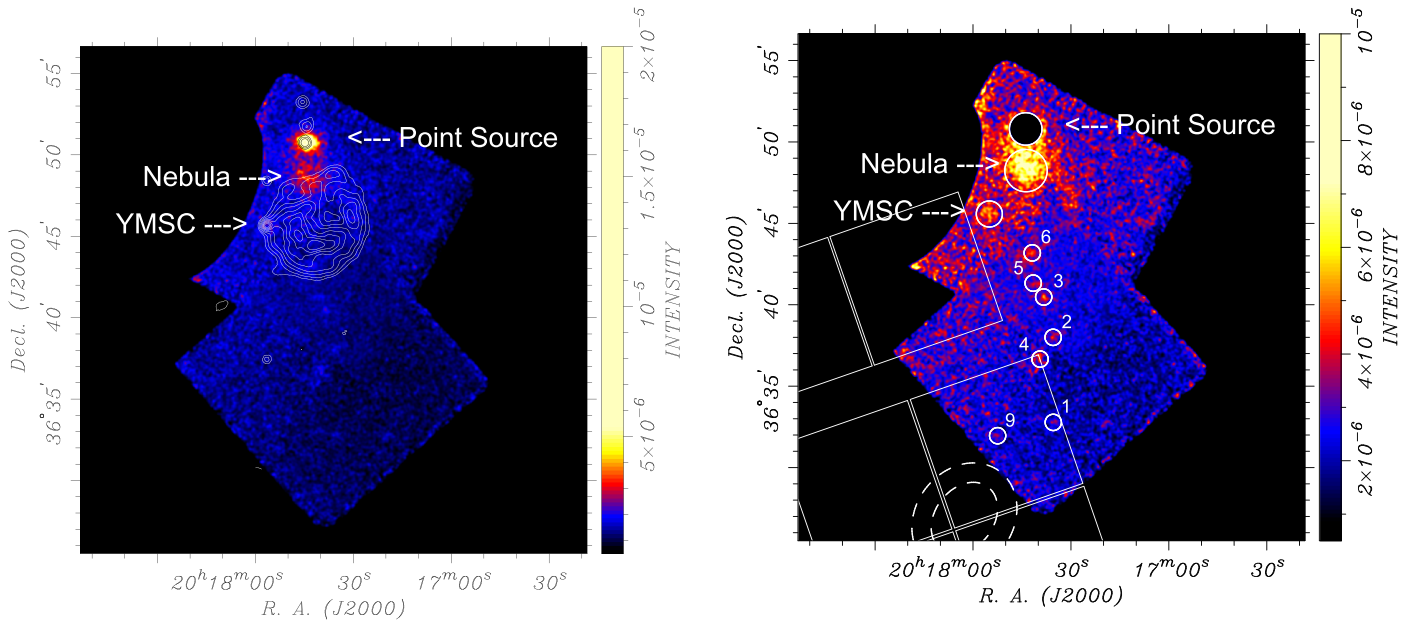
---

[12] http://heasarc.gsfc.nasa.gov/cgi-bin/Tools/w3nh/w3nh.pl

Figure 2. *NuSTAR* exposure-corrected and smoothed 3–79 keV X-ray images of the field containing Sh 2–104. (Left: a bright *NuSTAR* point source is evident up to 30 keV and a significant X-ray nebula is found in the 3–20 keV band just south of the point source. Both of these sources are of unknown origin. The nebula overlaps the rim of the H II region Sh 2–104, here outlined by the GMRT 610 MHz radio contours of Paredes et al. (2009). Faint hard X-ray emission is also seen at the location of the eastern YMSC enclosed by the radio spur. A bright arc on the edge of the image, due to stray light hitting the focal plane, has been excised. Right: the same image with the bright point source removed and scaled to highlight diffuse emission. Indicated (circles) are the detected *NuSTAR* sources listed in Table 1. Also shown is the location of the nearby *Chandra* observation (outline) of 3FGL J2017.9+3627 (contours).

Table 1
NuSTAR Sources in the Sh 2–104 Field

#	R.A.	Decl.	Net Counts	Sig. (Sigma)	Comment
1	20 17 35.97	+36 32 45.0	61 ± 14	4.4	⋯
2	20 17 36.02	+36 37 58.5	73 ± 16	5.2	*Swift* source
3	20 17 38.91	+36 40 27.1	45 ± 13	3.7	⋯
4	20 17 40.02	+36 36 38.3	24 ± 8	3.1	⋯
5	20 17 42.13	+36 41 18.2	50 ± 13	4.0	⋯
6	20 17 42.41	+36 43 09.7	48 ± 13	4.1	⋯
7	20 17 44.32	+36 48 12.9	2219 ± 82	27.0	Nebula *NuSTAR* J201744.3+364812
8	20 17 44.42	+36 50 46.4	1406 ± 54	35.0	3XMM J201744.7+365045
9	20 17 53.02	+36 31 56.0	52 ± 12	4.9	⋯
10	20 17 55.57	+36 45 33.1	197 ± 34	5.8	Sh 2–104 stellar cluster/HII region

Note. Coordinate system is registered to $\approx 4\rlap{.}''0$ accuracy using 3XMM J201744.7+365045, the counterpart to the bright *NuSTAR* point source.

from an adjacent aperture ($r < 1\rlap{.}'4$) on the same chip of each FPM. We consider several appropriate spectral models as the quality of the spectrum is not sufficient to distinguish between then. Under the assumption that the X-ray emission is due to colliding winds of component stars in the cluster we fit the Raymond thermal plasma model in XSPEC (Raymond & Smith 1977 and updates). The best-fit temperature is $kT = 1.2$–3.5 keV with a $\chi^2 = 1.1$ for 19 degrees of freedom (dof). The 2–10 keV unabsorbed flux is 1.7×10^{-13} erg cm^{-2} s^{-1}. We estimate a source luminosity of $L \sim 10^{33}$ erg s^{-1} from the plasma cooling curve (e.g., Maio et al. 2007) and the derived emission measure, computed from the model normalization and a distance of 4 kpc to Sh 2–104. We also consider a non-thermal model that can result from accelerated particles of past supernovae and/or quiescent or faint X-ray binaries. For a simple power-law model, the photon index is $\Gamma = 3.5(2.4$–$4.7)$ with a similar χ^2 and flux as found for the thermal model.

For 3XMM J201744.7+365045, we extracted a high-quality *NuSTAR* spectrum using an $r = 45'$ source aperture and an $r = 1\rlap{.}'4$ background region offset from the source. The source spectrum is found to dominate the background up to 20 keV, but emission is evident to at least 30 keV. The spectrum is well-fitted in the 3–20 keV energy band to an absorbed power-law model with the column density held fixed to the Galactic total. The best fit spectral index is $\Gamma = 2.0 \pm 0.1$ with $\chi^2 = 0.82$ for 28 dof. The unabsorbed flux in the 2–10 keV band is $(1.4 \pm 0.1) \times 10^{-12}$ erg cm^{-2} s^{-1}. A blackbody model is excluded by the fit as are, for the lack of line features, thermal plasma models. The spectral results are presented Table 2.

To better estimate the source column density for 3XMM J201744.7+365045 we extracted and fit the *XMM-Newton* spectrum simultaneously with the *NuSTAR* data, allowing the flux normalization to be independent. This resulted in $N_H = (3.1 \pm 1.0) \times 10^{22}$ cm^{-2} and spectral index $\Gamma = 2.1 \pm 0.1$ (see Figure 3). We note that the measured

Table 2
NuSTAR and *XMM-Newton* Spectra of 3XMM J201744.7+365045

Parameter	*NuSTAR* Only	*XMM-Newton* Only	*NuSTAR* + *XMM-Newton*[a]
N_H (cm^{-2})	2.4×10^{22} (fixed)	$3.4(1.8 - 5.6) \times 10^{22}$	$(3.1 \pm 1.0) \times 10^{22}$
Γ	2.0 ± 0.1	$1.4–3.1$	2.1 ± 0.1
F_{abs} (2–10 keV)	$1.2 \pm 0.1 \times 10^{-12}$	3.5×10^{-13}	$1.2 \pm 0.1 \times 10^{-12}$
F_{unabs} (2–10 keV)	1.3×10^{-12}	4.6×10^{-13}	1.4×10^{-12}
χ_ν^2 (dof)	0.82 (29)	0.68 (36)	0.70 (62)

Note. Power-law model fits are obtained in the 0.5–10 keV and 3–20 keV energy bands for the *XMM-Newton* and *NuSTAR* spectra, respectively. For the joint *NuSTAR* and *XMM-Newton* spectral fits, the indices and column densities are linked. The uncertainties are 90% confidence limits for two interesting parameters, except for the *NuSTAR*-only data, which are for one interesting parameter. The given fluxes are in units of erg cm^{-2} s^{-1}.

[a] The listed flux values are for the *NuSTAR* spectra, while the *XMM-Newton* spectra are jointly fit with a relative normalization factor to account for the flux variation.

column is consistent with our estimate of the Galactic total. Compared to the *XMM-Newton* flux measurements obtained 7 years earlier, the *NuSTAR* value is lower, formally by a factor of ∼3. However, the former flux is not well established due to poor statistics, the high background, and the far off-axis source detection on the edge of the *XMM-Newton* EPIC instruments, and the relative flux calibration between instruments.

To examine the X-ray nebula *NuSTAR* J201744.3+364812, we extracted spectra using a $r = 1\overset{\prime}{.}4$ radius aperture and the background region defined above. This aperture encompassed nearly all the nebula extent to the background level. Of the ∼3400 aperture counts in the 3–20 keV optimal energy band, ∼1400 (42%) are attributed to the background. A fit to the nebula spectrum using an absorbed power-law model in the 3–20 keV band with the total Galactic column density yields a photon index $\Gamma = 2.5$–2.8 with a $\chi_\nu^2 = 1.6$ for 57 dof. The 2–10 keV absorbed flux is $(6.4$–$7.5) \times 10^{-13}$ erg cm^{-2} s^{-1} (90% confidence level) and the unabsorbed flux is 8.7×10^{-13} erg cm^{-2} s^{-1}.

The poor χ^2 statistic for this fit is mainly due to a line-like feature around 5.6 keV (see Figure 4). No similar feature appears in the background or the *NuSTAR* spectrum of the point source 3XMM J201744.7+365045. Introducing a Gaussian line to the fit, to better characterize the continuum, yield a line measured at 5.6 ± 0.2 keV and results in an excellent fit statistic of $\chi_\nu^2 = 0.94$ for 54 dof. The F-test value of 13.09 corresponds to a false positive significance of the added spectral line of $\wp = 2.3 \times 10^{-5}$. However, this significance should be interpreted with care (Protassov et al. 2002). Formally, an analysis of the F-test probability using the XSPEC script simftest confirms a highly significant detection of an emission line feature associated with the source.

As no emission line is known at this energy we consider the possibility of a redshifted Fe line from a galaxy cluster hidden behind the Galactic plane. A spectral fit using the Raymond-Smith model for a thermal plasma produced an excellent fit again, with $\chi_\nu^2 = 0.86$ for 55 dof, with the column density fixed at the Galactic total. The best-fit parameters give a $kT = 5.6^{+1.3}_{-0.83}$ keV, redshift $z = 0.19 \pm 0.02$, and abundance $0.66 \, Z_\odot$. The 2–10 keV absorbed flux is $6.4^{+0.3}_{-0.6} \times 10^{-13}$ erg cm^{-2} s^{-1} (90% confidence level) and the unabsorbed flux is 7.5×10^{-13} erg cm^{-2} s^{-1}. We note that the measured range of kT is essentially independent of the column density, from zero to 3.1×10^{22} cm^{-2}, the point source value. This N_H range yields a measured temperature range of $kT = 5.3$–6.4 keV, comparable to the uncertainty in kT obtained using the Galactic column.
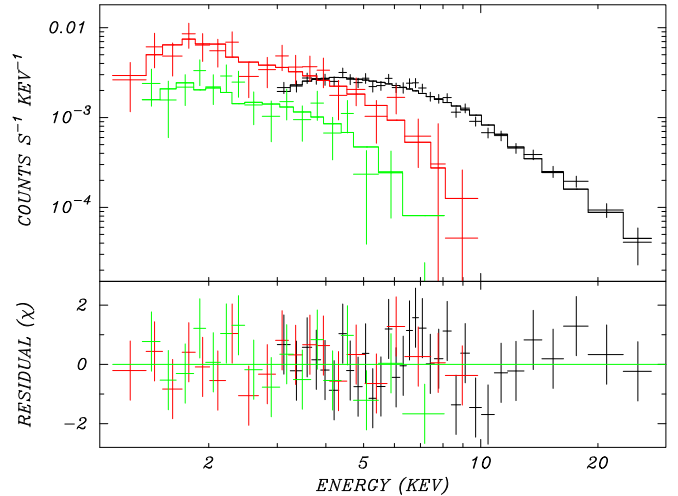

Figure 3. *NuSTAR* and *XMM-Newton* spectra of 3XMM J201744.7+365045. The spectra are fitted simultaneously to an absorbed power-law model with their normalizations left free. The upper panel presents *NuSTAR* (black) and *XMM-Newton* EPIC pn (red) and EPIC MOS (green) spectral histograms along with the best-fit model (solid lines) given in Table 2. The lower panel shows the residuals from the best-fit model in units of sigma.

For a galaxy cluster at the implied redshift distance of 800 Mpc, the total X-ray luminosity is $L_x = 1.2 \times 10^{44}$ erg s^{-1}. This is within an order of magnitude of the value derived from the luminosity—temperature relation for clusters (Novicki et al. 2002). Moreover, based on the inferred temperature, the observed nebula size is well predicted for a putative cluster (Mohr et al. 2000). Given the large uncertainties in these relations we take the results as reasonable evidence that the X-ray nebula is due to a background galaxy cluster unrelated to the gamma-ray emission.

2.3. Timing Analysis

The high time resolution of *NuSTAR* allows a search for pulsations from 3XMM J201744.7+365045 down to periods of $P \sim 4$ ms, covering the expected range for a rotation-powered pulsar. For a timing analysis, photon arrival times were converted to barycentric dynamical times using the *XMM-Newton* coordinates. The *NuSTAR* light curve is found to be stable during the observation on all timescales. A fast Fourier transform (FFT) finds no evidence of red noise, indicative of accreting systems in the power spectrum. We also searched for a coherent signal using both the FFT method and the Z_n^2 test statistic for $n = 1, 2, 3, 5$, and the H-test, to be sensitive to both broad and narrow pulse profiles. We initially restricted the
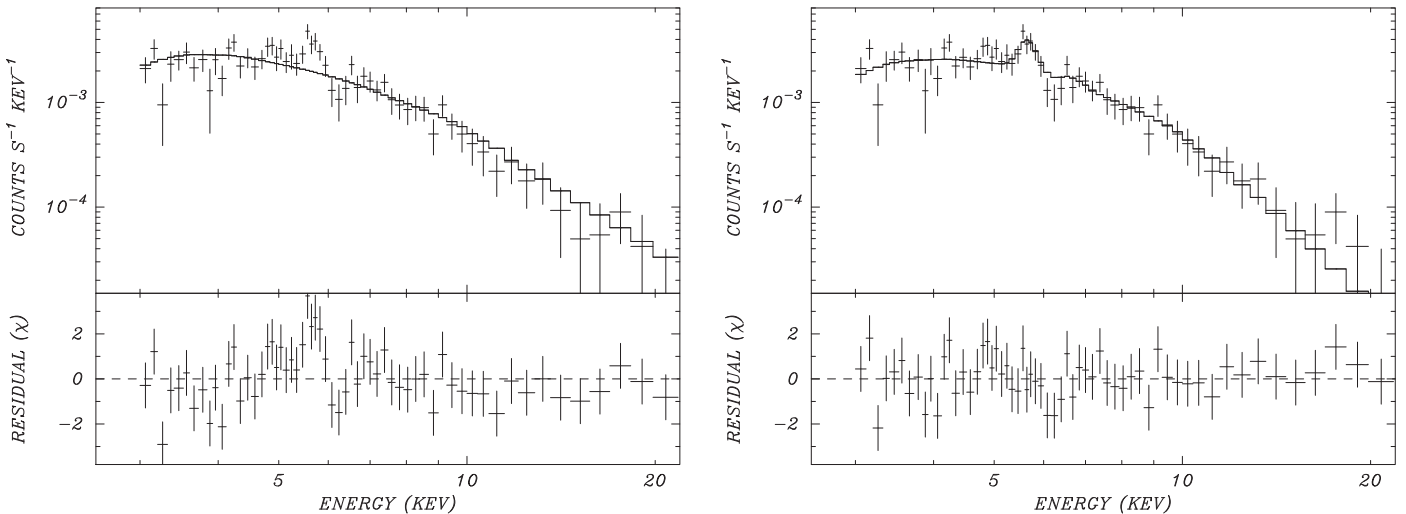
Figure 4. *NuSTAR* spectra of the new X-ray nebula *NuSTAR* J201744.3+364812. Left—the spectrum fitted with an absorbed power-law (solid lines). The lower panel shows the residuals from the best-fit model given in the text, in units of sigma. Right—the same spectrum fitted with the addition of an emission line.

timing search to photon energies in the 3–25 keV range and used an aperture of 30′ to optimize the signal-to-noise ratio. We repeated our search for an additional combination of energy ranges $3 < E < 10$ keV and $10 < E < 25$ keV, and aperture sizes $r > 10'$. None of these resulted in a significant detection. After taking into account the estimated background emission, we place an upper limit on the pulse fraction $f_p \leqslant 43\%$ for a sinusoidal signal in the 3–25 keV band for the 20′ aperture.

3. DISCUSSION

TeV gamma-ray emission from MGRO J2019+37 is well-separated into three regions by high-resolution VERITAS observations, each associated with a *Fermi* source (Aliu et al. 2014). To the north, VER J2016+371 is likely associated with *Fermi* emission from the blazar B2013+370 (Kara et al. 2012) and/or the filled-center supernova remnant CTB 87 (Aliu et al. 2014). To the south, localized VERITAS excess, significant at the 3σ confidence level is a coincident with the recently discovered *Fermi* pulsar, PSR J2017+3627, discussed below. To the east, the large elliptical morphology of the spectrally harder VER J2019+368 suggests a blend of two overlapping sources. If the arguments of Paredes et al. (2009) are correct, the *Fermi* pulsar PSR J2021+3651 easily accounts for the eastern most TeV emission from VER J2019+368, while Sh 2–104 may be responsible for a western component. In the following, we use new X-ray observations to explore possible origins for an eastern component of VER J2019+368.

The *NuSTAR* data reveals faint emission from the eastern YMSC of Sh 2–104, with an inferred luminosity of $L \sim 10^{33}$ erg s^{-1}. In other young massive stellar clusters, hard >3 keV X-rays have been seen at similar levels from either point sources (Clark et al. 2008) or diffuse emission (Townsley et al. 2011). For the point source case, although it is possible for hard X-rays to be produced by an accreting compact object, a small number of isolated OB supergiants or Wolf-Rayet stars, colliding wind binaries (CWBs), or possibly even a single CWB could produce hard X-ray emission at the levels we observe (Clark et al. 2008; Sugawara et al. 2015). If a thermal model is the correct characterization of the *NuSTAR* spectrum, then the plasma temperature of ~2–3 keV would favor CWBs over isolated massive stars (Bodaghee et al. 2015; Sugawara

et al. 2015). Diffuse thermal or non-thermal X-ray emission could come from particles accelerated by past supernova events or continuous acceleration in CWB shocks (Muno et al. 2006; Townsley et al. 2011). Townsley et al. (2011) report non-thermal diffuse emission from NGC 3576 N with a power-law spectrum with $\Gamma < 2.5$. The power-law fit to Sh 2–104 YMSC gives $\Gamma = 3.5^{+1.2}_{-1.1}$, which is just barely compatible with NGC 3576 N.

The coincidence of gamma-ray emission near star-forming regions suggests a physical connection between the two—for example, W49A (Brun et al. 2010), Westerlund1 (Luna et al. 2010), and Carina Nebula, although the gamma-rays from the latter are likely dominated by the CWB η Carinae (Tavani et al. 2009; Farnier et al. 2011). However, this connection remains far from clear, at least on an individual basis. For the case of the YMSC in Sh 2–104, we can consider several plausible physical mechanisms for generating the associated gamma-rays. As mentioned above, it is unlikely that the massive star binaries and protostars in the YMSC are sufficiently energetic to power a significant fraction of the TeV flux from the Milagro source, which is likely hadronic in nature, if extended. However, the YMSC may contribute gamma-rays to the western compact component of VER J2019 +368, via a leponic process. This reduces the required energy budget by about two orders of magnitude (see Paredes et al. 2009).

The YMSC could also host other young and powerful non-thermal sources associated with massive stars, such as high-mass microquasars or massive binaries containing non-accreting pulsars (e.g. Dubus 2013; Paredes et al. 2013). These sources, potentially hidden in hard X-rays by the dense environment in which they would be embedded, could also contribute to the overall gamma-ray emission from VER J2019 +368. Qualitatively, if only a fraction of the source flux came from the YMSC, for example a third, the energetic require-ments of the western component of VER J2019+368 would be reduced, and a hadronic mechanism may be plausible. Then the lack of associated GeV emission from VER J2019+368 could be explained by hadronic models for which the lower energy emission is suppressed, e.g., proton–proton interactions in the innermost region of the winds of massive O and B stars, as

suggested by Torres et al. (2004; see also Aharonian & Atoyan 1996; Bosch-Ramon et al. 2005) for scenarios in which the GeV emission is rather low as compared to the TeV emission).

Alternatively, the substantial X-ray emission that lies outside the radio nebula of Sh 2–104 perhaps signals a previously unidentified star cluster responsible for the TeV emission. However, no specific optical or infrared counterpart is known. The coordinates of 3XMM J201744.7+365045 are consistent to within $1''1$ with the 20 cm arcsec radio point source G74.840 +0.660 (FIRST Radio Survey; White et al. 2005), possibly the 327 MHz source WSRTGP 2015+3641 (Taylor et al. 1996), both non-descript radio objects in these Galactic surveys. A dedicated radio observation of Cygnus at 610 MHz by Paredes et al. (2009) determined a flux density of 33.46 ± 0.08 mJy for GMRT J201744.8+365045. Comparing this to the 20 cm flux of 11.15 mJy (White et al. 2005) yields a spectral index of $\alpha = 1.2$, where $F_\nu = \nu^{-\alpha}$.

The combination of the radio and X-ray point source and diffuse emission suggests a pulsar and its wind nebula, perhaps born in the star formation region, which provide a natural source of seed photons for generating upscattered gamma-rays (cf., HESS J1837–069/PSR J1838–0655; Gotthelf & Halpern 2008). Although the offset between the point source and the nebula is somewhat unusual, PWN systems often show complex X-ray morphology, as revealed by *Chandra* (e.g., Crab, MSH 15−52; see Kargaltsev & Pavlov 2008).

The X-ray spectrum of 3XMM J201744.7+365045 is, however, somewhat steep for a pulsar, more consistent with that of a hidden optical AGN behind the Galactic plane. The radio spectrum also prefers an AGN interpretation over a pulsar. The likely coincidence with a bright point-like radio source, the lack of detected pulsations (>43%), and the possible long-term variability, strengthen this interpretation. However, it is worth noting that the upper limit on the modulation for an X-ray pulsar is not strongly constraining.

The origin of the nebula NuSTAR J201744.3+364812 and whether it is connected to the point source remain a mystery. The appearance of a possible spectral line at an unexpected energy suggests that this feature, if astrophysical, is likely a redshifted Fe line from a galaxy cluster hidden behind the Galactic plane. The estimated luminosity and size of the nebula, based on its implied redshift and temperature, is consistent with this interpretation. The large column in the region (e.g., ∼19 magnitude of extinction in the V-band) could easily account for the lack of an optical counterpart.

Finally, it is possible that the TeV gamma-ray emission near Sh 2–104 might be associated with the *Fermi* source 3FGL J2017.9+3627, $0°3$ to the south of the H II region. A search for pulsations from 3FGL J2017.9+3627 by the Einstein@Home distributed computing pulsar project (Anderson et al. 2006; Allen et al. 2013) detected a 167 ms signal, consistent with a 2 Myr old rotation-powered pulsar (Clark 2016, ApJ, submitted).[13] The inferred spin-down power of PSR J2017+3625, $\dot{E} = 1.2 \times 10^{34}$ erg s^{-1}, suggests that it likely lies at a distance of 450 pc, given its gamma-ray flux of 4.8×10^{-11} erg s^{-1} cm^{-2} (Acero et al. 2015) and a gamma-ray efficiency of $L_{\mathrm{GeV}}/\dot{E} = 0.1$, typical for a *Fermi* pulsar. On the other hand, the lack of significant X-ray detection of a candidate NS in the unpublished 10 ks *Chandra* observation (ObsID 14699) suggests that the pulsar is further away. For this

observation, we estimate a flux limit of F_x (2–10 keV) $\lesssim 2 \times 10^{-14}$ erg s^{-1} cm^{-2} for a typical pulsar power-law spectrum ($N_{\mathrm{H}} = 1.0 \times 10^{22}$ cm^{-2}; $\Gamma = 1.5$). The predicted distance is then $\gtrsim 1$ kpc, based on the empirical relation between the X-ray luminosity of pulsars and their spin-down power (Possenti et al. 2002). At this distance, the local TeV emission, estimated to be roughly L (1–10 TeV) $\sim 3 \times 10^{-12}$ erg s^{-1}, represents an efficiency of $L_{\mathrm{TeV}}/\dot{E} \sim 0.03$, plausible for a $>10^5$ years pulsar (e.g., see Kargaltsev et al. 2013).

In conclusion, it is possible that PSR J2017+3625 accounts for most, if not all, of the coincident VERITAS TeV excess and that the harder TeV photons near Sh 2–104 remain unaccounted for. Our analysis of the X-ray data is inconclusive as to the connection between the *NuSTAR* sources, the Sh 2–104 region, and the overlapping gamma-ray emission. Without further evidence, it is not yet possible to associate the Milagro gamma-ray emission with Sh 2–104. In this regard, it is important to determine the nature of the *NuSTAR* sources presented in this study. This will require high-resolution *Chandra* observations to allow a comparison between these sources and several overlapping optical/IR stars and an unclassified radio source, which may or may not be related to the X-ray and/or gamma-ray emission.

REFERENCES

Abdo, A. A., Allen, B., Berley, D., et al. 2007, ApJL, 658, L33
Acero, F., Ackermann, M., Ajello, M., et al. 2015, ApJS, 218, 23
Aharonian, F. A., & Atoyan, A. M. 1996, A&A, 309, 917
Aliu, E., Aune, T., Behera, B., et al. 2014, ApJ, 788, 78
Allen, B., Knispel, B., Cordes, J. M., et al. 2013, ApJ, 773, 91
Anderson, D. P., Christensen, C., & Allen, B. 2006, in Proc. of the 2006 ACM/IEEE Conf. on Supercomputing, SC '06 (New York: ACM)
Arnaud, K. A. 1996, in ASP Conf. Ser. 101, Astronomical Data Analysis Software and Systems V, ed. G. H. Jacoby, & J. Barnes (San Francisco, CA: ASP), 17 (http://www.aspbooks.org/a/volumes/article_details/?paper_id=12588)
Bodaghee, A., Tomsick, J. A., Fornasini, F., Rahoui, F., & Bauer, F. E. 2015, ApJ, 801, 49
Bosch-Ramon, V., Aharonian, F. A., & Paredes, J. M. 2005, A&A, 432, 609
Brun, F., de Naurois, M., Hofmann, W., et al. 2010, in Proc. 25th Texas Symposium on Relativistic Astrophysics, ed. F. M. Rieger, C. van Eldik, &

---

[13] https://einstein.phys.uwm.edu/gammaraypulsar/gFGRP1_discoveries.html

W. Hofmann (Heidelberg, Germany: SOC), 123 (http://pos.sissa.it/cgi-bin/reader/conf.cgi?confid=123, id.201)

Clark, C. 2016, ApJ, submitted

Clark, J. S., Muno, M. P., Negueruela, I., et al. 2008, A&A, 477, 147

Dame, T. M., Hartmann, D., & Thaddeus, P. 2001, ApJ, 547, 792

Deharveng, L., Lefloch, B., Zavagno, A., et al. 2003, A&A, 408, L25

Dubus, G. 2013, ARA&A, 21, 64

Farnier, C., Walter, R., & Leyder, J.-C. 2011, A&A, 526, A57

Gotthelf, E. V., & Halpern, J. P. 2008, ApJ, 681, 515

Harrison, F. A., Craig, W. W., Christensen, F. E., et al. 2013, ApJ, 770, 103

Kara, E., Errando, M., Max-Moerbeck, W., et al. 2012, ApJ, 746, 159

Kargaltsev, O., & Pavlov, G. G. 2008, in AIP Conf. Ser. 983, 40 Years of Pulsars: Millisecond Pulsars, Magnetars and More, ed. C. Bassa et al. (Melville, NY: AIP), 171

Kargaltsev, O., Rangelov, B., & Pavlov, G. G. 2013, arXiv:1305.2552

Lahulla, J. F. 1985, A&AS, 61, 537

Luna, A., Mayya, Y. D., Carrasco, L., & Bronfman, L. 2010, ApJL, 713, L45

Madsen, K. K., Harrison, F. A., Markwardt, C. B., et al. 2015, ApJS, 220, 8

Maio, U., Dolag, K., Ciardi, B., & Tornatore, L. 2007, MNRAS, 379, 963

Mohr, J. J., Reese, E. D., Ellingson, E., Lewis, A. D., & Evrard, A. E. 2000, ApJ, 544, 109

Mori, K., Gotthelf, E. V., Dufour, F., et al. 2014, ApJ, 793, 88

Muno, M. P., Law, C., Clark, J. S., et al. 2006, ApJ, 650, 203

Novicki, M. C., Sornig, M., & Henry, J. P. 2002, AJ, 124, 2413

Paredes, J. M., Martí, J., Ishwara-Chandra, C. H., et al. 2009, A&A, 507, 241

Paredes, J. M., Bednarek, W., Bordas, P., et al. 2013, APh, 43, 301

Possenti, A., Cerutti, R., Colpi, M., & Mereghetti, S. 2002, A&A, 387, 993

Protassov, R., van Dyk, D. A., Connors, A., Kashyap, V. L., & Siemiginowska, A. 2002, ApJ, 571, 545

Raymond, J. C., & Smith, B. W. 1977, ApJS, 35, 419

Roberts, M. S. E., Hessels, J. W. T., Ransom, S. M., et al. 2002, ApJL, 577, L19

Sugawara, Y., Maeda, Y., Tsuboi, Y., et al. 2015, PASJ, 67, 121

Tavani, M., Sabatini, S., Pian, E., et al. 2009, ApJL, 698, L142

Taylor, A. R., Goss, W. M., Coleman, P. H., van Leeuwen, J., & Wallace, B. J. 1996, ApJS, 107, 239

Torres, D. F., Domingo-Santamaría, E., & Romero, G. E. 2004, ApJL, 601, L75

Townsley, L. K., Broos, P. S., Chu, Y.-H., et al. 2011, ApJS, 194, 16

Verner, D. A., Ferland, G. J., Korista, K. T., & Yakovlev, D. G. 1996, ApJ, 465, 487

White, R. L., Becker, R. H., & Helfand, D. J. 2005, AJ, 130, 586

Wilms, J., Allen, A., & McCray, R. 2000, ApJ, 542, 914

Zabalza, V., Paredes, J. M., Martí, J., Sánchez-Sutil, J. R., & Muñoz-Arjonilla, A. J. 2010, in ASP Conf. Ser. 422, High Energy Phenomena in Massive Stars, ed. J. Martí, P. L. Luque-Escamilla, & J. A. Combi (San Francisco, CA: ASP), 186